Electronic Supplementary Information (ESI) for:

Metal-organic framework nanoparticles for arsenic trioxide drug delivery

Romy Ettlinger,[a] Marthe Sönksen,[b] Monika Graf,[b] Natalia Moreno,[b] Dmytro Denysenko,[a] Dirk Volkmer,[a] Kornelius Kerl [b] and Hana Bunzen[a]*

[a] Chair of Solid State and Materials Chemistry, Institute of Physics, University of Augsburg, Universitätsstraße 1, D-86159 Augsburg, Germany
[b] University Children´s Hospital Muenster, Pediatric Hematology and Oncology, Albert-Schweitzer-Campus 1, D-48149 Muenster

Contents

Characterization of MFU-4*l*, MFU-4*l*-OAs(OH)$_2$ and PEG@MFU-4*l*-OAs(OH)$_2$	S2
Computational modelling	S6
Drug release and MOF stability studies	S10
Cytotoxicity studies	S17
References	S17

Characterization of MFU-4*l*, MFU-4*l*-OAs(OH)$_2$ and PEG@MFU-4*l*-OAs(OH)$_2$

Transmission electron microscopy (TEM)

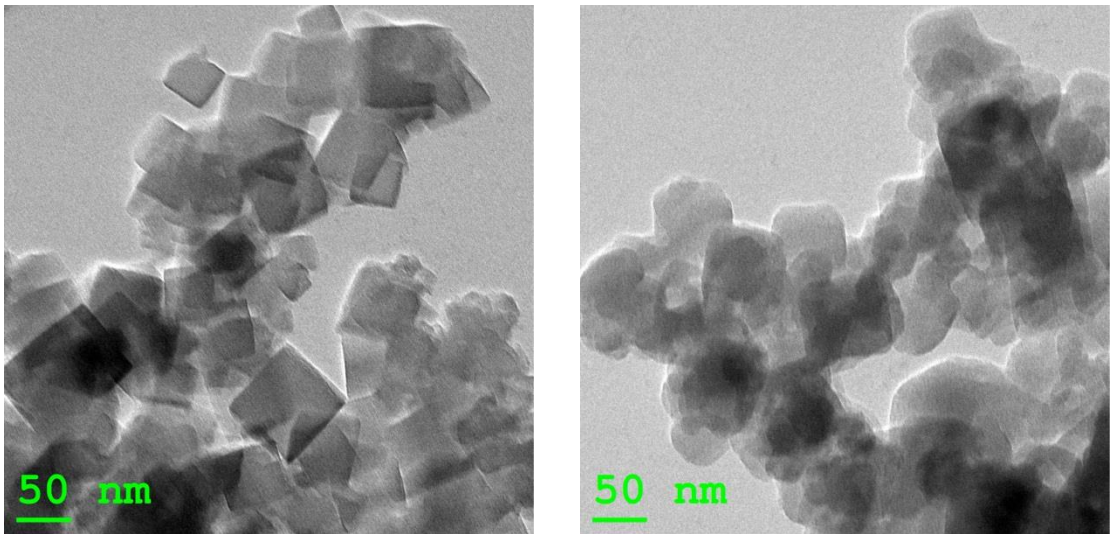

Fig. S1 TEM micrograph of MFU-4*l* nanoparticles before (left) and after (right) the drug loading; scale bar: 50 nm.

Dynamic light scattering (DLS) measurements

Table S1 DLS data of non-coated and PEG-coated MFU-4*l* nanoparticles dispersed in distilled water. The data are presented as a median for number distributions (Dn50) with a polydispersity index (PDI) shown in parentheses. After less than 24 hours, the non-coated nanoparticles start to agglomerate, while the functionalized particles retain their colloidal stability.

Time	Non-coated nanoparticles Dn50 (PDI)	PEG-coated nanoparticles Dn50 (PDI)
After dispersion	116.1 nm (0.229)	109.0 nm (0.220)
After 2 h	119.2 nm (0.218)	110.5 nm (0.209)
After 4 h	118.2 nm (0.219)	106.9 nm (0.206)
After 24 h	270.6 nm (0.332)	107.0 nm (0.228)
After 48 h	> 500 nm	111.6 nm (0.218)

Sorption analysis

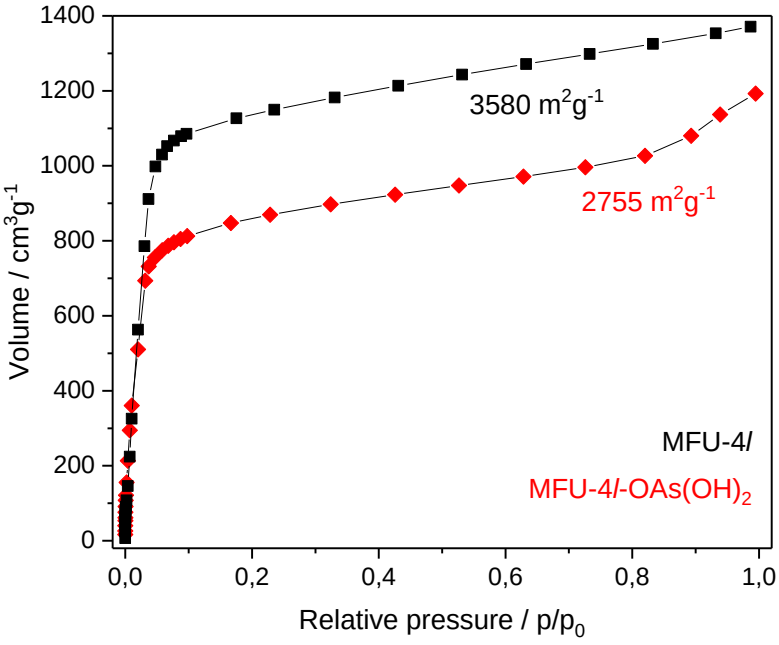

Fig. S2 Argon adsorption isotherms for MFU-4*l* (black) and MFU-4*l*-OAs(OH)$_2$ (red) at 77 K.

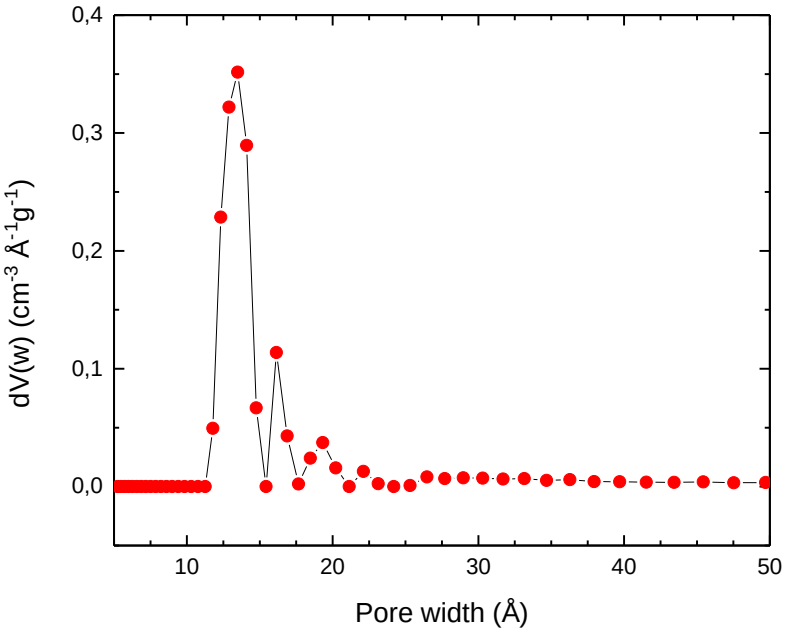

Fig. S3 Pore size distribution for MFU-4*l*-OAs(OH)$_2$ calculated by fitting NLDFT models to the argon adsorption data.

Variable temperature X-ray powder diffraction (VT XRPD)

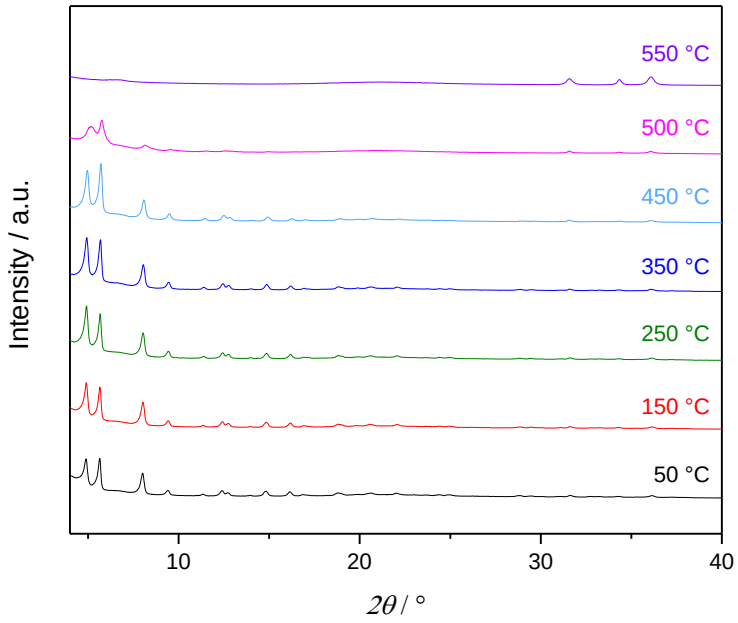

Fig. S4 VT XRPD patterns of MFU-4*l*-OAs(OH)$_2$ in the range of 50-550 °C (sample exposed to a flow of nitrogen gas).

Thermogravimetric analysis

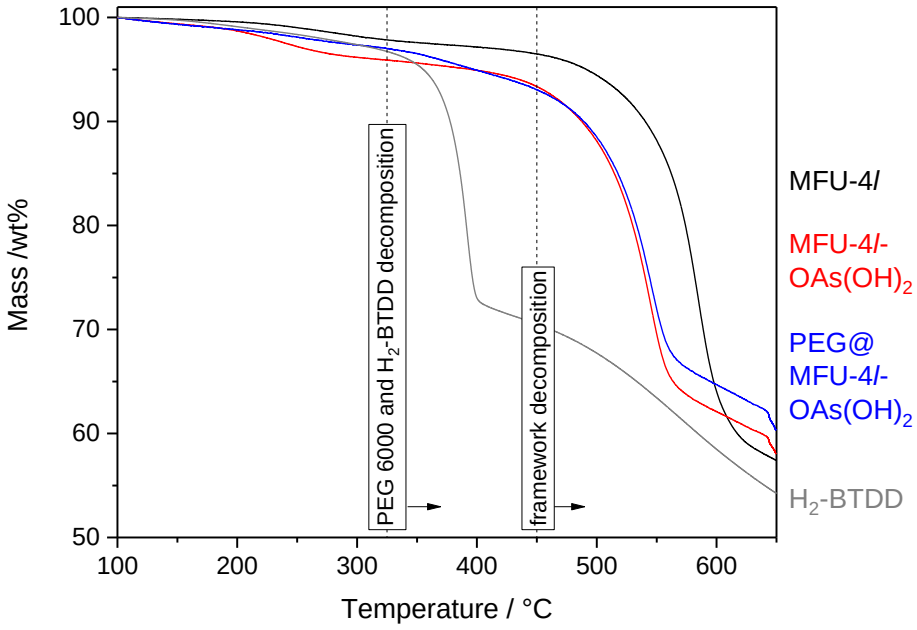

Fig. S5 Thermogravimetric analysis of activated MFU-4*l* nanoparticles (black), MFU-4*l*-OAs(OH)$_2$ (red), PEG@MFU-4*l*-OAs(OH)$_2$ nanoparticles (blue) and H_2-BTDD (grey) (sample exposed to a flow of nitrogen gas).

FTIR spectroscopy

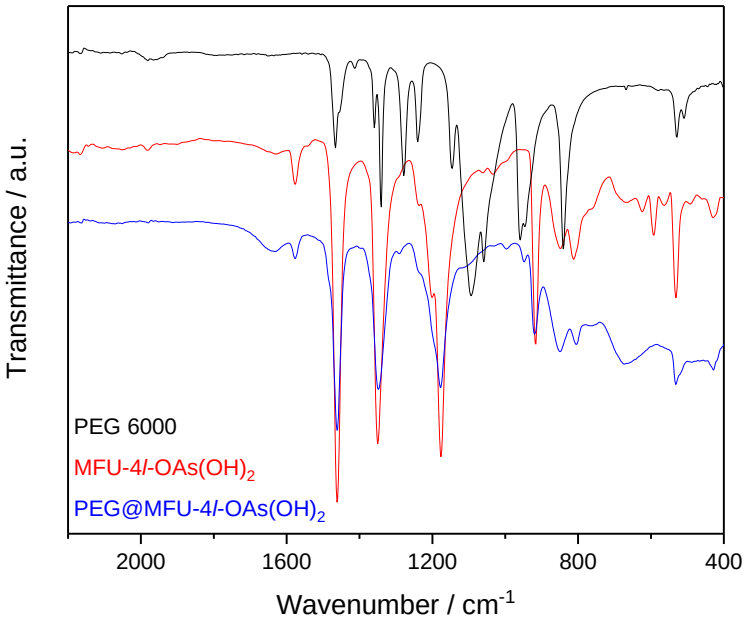

Fig. S6 Comparison of IR spectra of PEG 6000 (black), MFU-4*l*-OAs(OH)$_2$ (red) and PEG@MFU-4*l*-OAs(OH)$_2$ (red) in the area from 2200 to 400 cm^{-1}.

Computational modelling

Model complexes

DFT calculations on model complexes (which feature zinc ions in a tetrahedral coordination environment structurally related to the zinc ions found in the secondary building unit of MFU-4*l*), were performed with DMol^3 as part of BIOVIA Materials Studio Rel. 2018.[1,2] The geometry of complexes were fully refined [PBE-GGA, spin restricted all-electron numerical DNP basis set (4.4. basis file)]. The models included [ZnCl(Tp)] (Tp = trispyrazolylborate ligand) and [Zn(OAs(OH)$_2$)(Tp)] featuring three different arsenite binding modes (including a tautomeric Zn-As-bound species, Fig. S7). Vibrational frequencies were obtained from geometrical displacement calculations on fully converged models. All models were lacking imaginary (negative) frequencies. Thermodynamic properties were calculated from frequency analysis, allowing to compare the relative energies of the three different arsenite coordination modes.

Table S2 Comparison of the total energy E_t and enthalpy of [ZnCl(Tp)] and [Zn(OAs(OH)$_2$)(Tp)] with three different arsenite binding modes.

Model	Total energy E_t / Ha	Enthalpy (298.15 K incl. ZPVE) / kcal mol^{-1}
[ZnCl(Tp)]	-2941.1548339	134.805
Model A: [Zn(-As(=O)(OH)$_2$(Tp)]	-4943.452746	156.074
Model B: [Zn(O-AsH(=O)(-OH)(Tp)]	-4943.437371	155.739
Model C: [Zn(O-As(-OH)$_2$)(Tp)]	-4943.484229	156.340

The structural Model C was found to be the most stable among the modelled different arsenite-bound complexes. Therefore, this coordination mode was transferred into a 3D periodic model of arsenite exchanged MFU-4*l*.

Model A	Model B	Model C
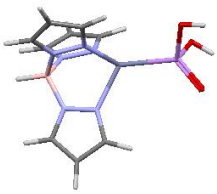	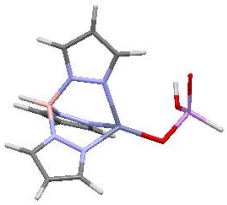	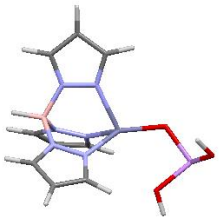

Fig. S7 Modelled structures of [Zn(OAs(OH)$_2$)(Tp)] with three different arsenite binding modes (Model A, B and C).

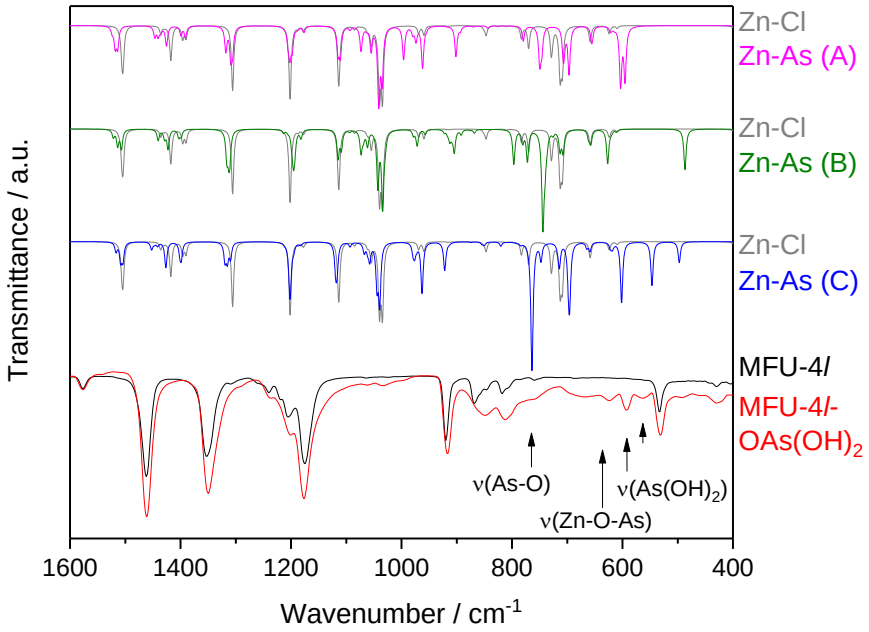

Fig. S8 Modelled FTIR spectra of the [Zn(OAs(OH)$_2$)(Tp)] complexes: A (magenta), B (green) and C (blue) in comparison to measured FTIR spectra of MFU-4*l* (black) and MFU-4*l*-OAs(OH)$_2$ (red) in the area from 1600 to 400 cm^{-1}.

Periodic lattice model calculations

A DFT calculation on an arsenite-exchanged 3D periodic lattice model of MFU-4*l*-(O-As(-OH)$_2$) was performed with CASTEP as part of BIOVIA Materials Studio Rel. 2018.[3] The geometry of the crystal lattice was fully optimized employing plane-wave DFT calculations (PBE-GGA, norm-conserving pseudo potentials with a plane wave basis set energy cut-off at 830 eV). Calculations were performed on the primitive of a body-centered tetragonal cell within space group *I* 4/*m* (no. 87). The tetragonal setting was supposed to represent the highest possible crystallographic symmetry of arsenite-exchanged MFU-4*l*, which itself crystallizes in a cubic crystal system (space group *F* $m\bar{3}m$, no. 225). Selected properties of the tetragonal cell of MFU-4*l*-(O-As(-OH)$_2$) are shown in Table S3. A cif file of the converged structure is provided as part of the supplementary material. Vibrational frequencies were obtained from linear response calculations on the fully converged lattice model. Selected calculated frequencies are presented in Table S2 together with an assignment to characteristic (localized = vibrational modes).

Table S3 Additional vibrational frequencies observed in the modelled IR spectrum of MFU-4*l*-OAs(OH)$_2$ in comparison to the modelled IR spectrum of MFU-4*l* (both shown in Fig. S9).

Vibrational frequency / cm^{-1}	Vibrational mode
480	H-O-As angular deformation
579, 616, 617	(HO)-As stretching
784	Zn-As stretching
940, 950	As-O-H combination tone
1235	C-H-linker deformation
3067	C-H-stretching
3575, 3598	O-H-stretching (AsOH)

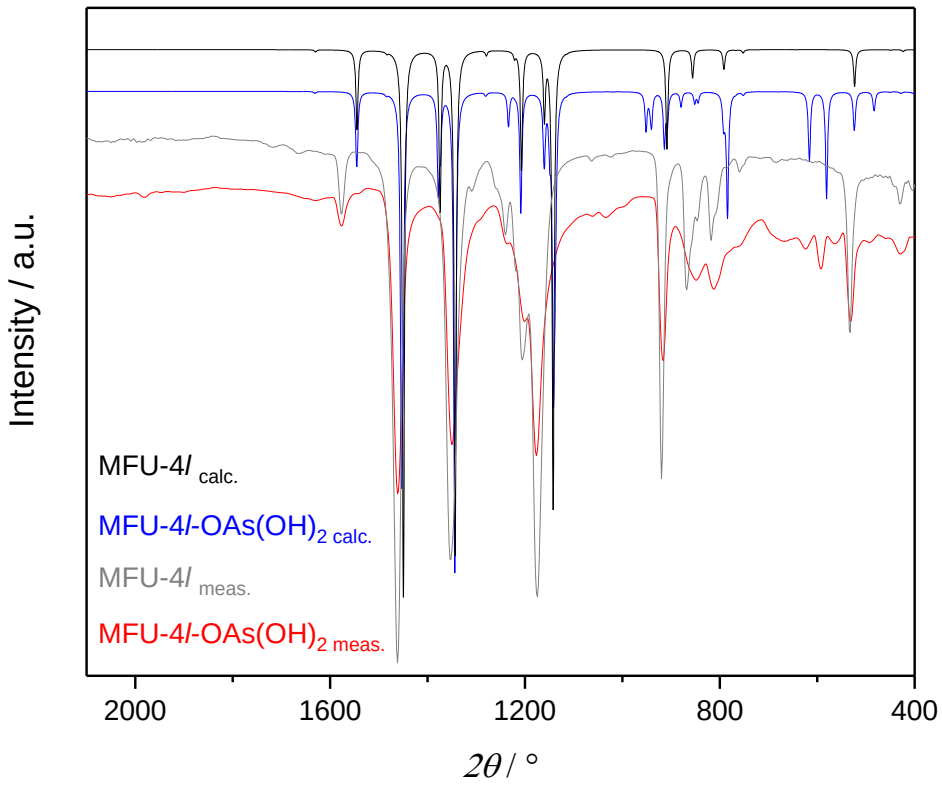

Fig. S9 Comparison of modelled IR spectra of MFU-4*l* and MFU-4*l*-OAs(OH)$_2$ (black, blue) with measured FTIR spectra of MFU-4*l* and MFU-4*l*-OAs(OH)$_2$ (red, grey) in the area from 2100 to 400 cm^{-1}.

Table S4 Summary of the crystal structure data of MFU-4*l* and MFU-4*l*-OAs(OH)$_2$.

	MFU-4*l* measured	MFU-4*l*-OAs(OH)$_2$ simulated
Chemical formula	$C_{36}Cl_4N_{18}H_{12}O_6Zn_5$	$As_4C_{36}N_{18}H_{20}O_{18}Zn_5$
Formula weight / g mol^{-1}	1261.32	1619.39
Crystal system	cubic	tetragonal
Space group	*F* $m\bar{3}m$ (no. 225)	*I* 4/*m* (no. 87)
a / Å	31.0569	22.3607
c / Å		31.9284
V / Å^3	29955.2	15964.23^3

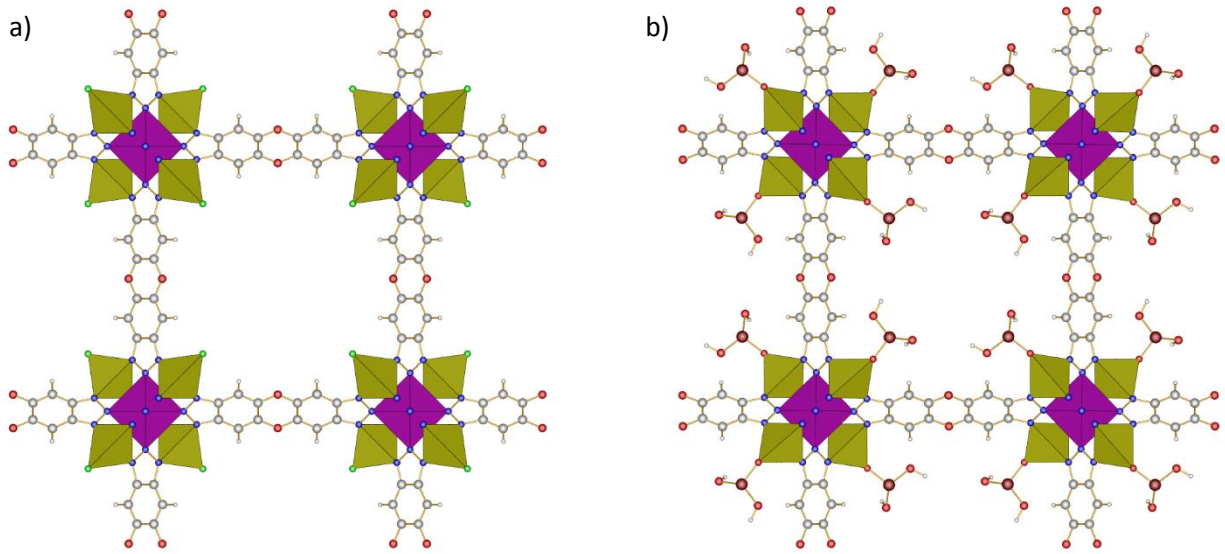

Fig. S10 Comparison of the crystal structure of MFU-4*l* (a) and MFU-4*l*-OAs(OH)$_2$ (b).
(C: grey; H: white; O: red; N: blue; Cl: green; Zn-octahedral: purple; Zn-tetrahedral: yellow; As: dark red)

Drug release and MOF stability studies

Drug release followed over 7 days

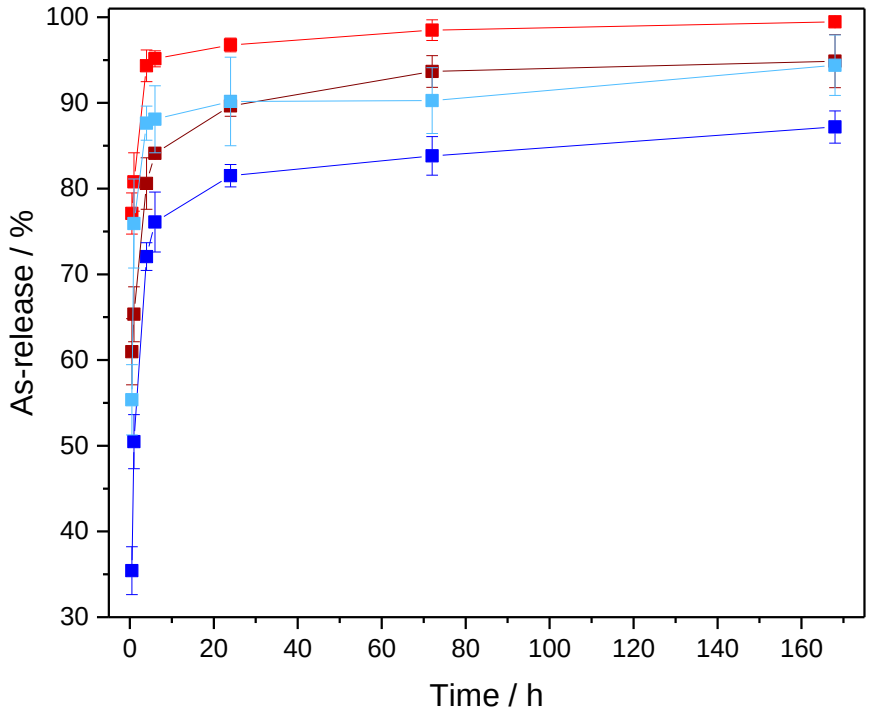

Fig. S11 Arsenic release from MFU-4*l*-OAs(OH)$_2$ and PEG@MFU-4*l*-OAs(OH)$_2$ at pH 6 (red, light blue) and pH 7.4 (dark red, dark blue) in a phosphate buffer solution at 37 °C, determined by ICP-OES.

Table S5 Amount of arsenic (%) released from MFU-4*l*-OAs(OH)$_2$ and PEG@MFU-4*l*-OAs(OH)$_2$ into a phosphate buffer solution at 37 °C at pH 6 and pH 7.4, determined by ICP-OES.

Time	pH 6	pH 6 (PEG coated)	pH 7.4	pH 7.4 (PEG coated)
0.5 h	77.1 ± 2.4	55.4 ±. 4.1	60.9 ± 3.8	35.4 ± 2.8
1 h	80.8 ± 3.4	75.9 ± 5.1	65.3 ± 3.2	50.5 ± 3.2
4 h	94.3 ± 1.8	87.6 ± 2.0	80.6 ± 3.0	72.0 ± 1.6
6 h	95.1 ± 0.9	88.1 ± 3.9	84.1 ± 0.7	76.1 ± 3.5
24 h	96.8 ± 0.8	90.2 ± 4.9	89.6 ± 1.2	81.5 ± 1.3
72 h	98.5 ± 1.2	90.3 ± 3.8	93.7 ± 1.8	83.8 ± 2.2
168 h	99.5 ± 0.5	94.4 ± 3.5	94.9 ± 3.0	87.2 ± 1.8

MOF stability in phosphate buffered saline followed over 7 days

FTIR spectroscopy:

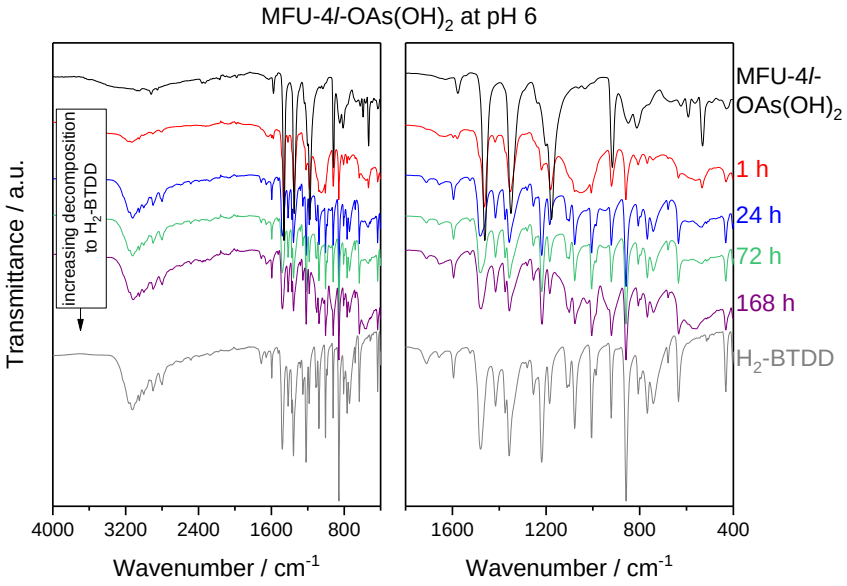

Fig. S12 FTIR spectra of MFU-4*l*-OAs(OH)$_2$ (black) and MFU-4*l*-OAs(OH)$_2$ after the arsenic release studies carried out at pH 6 for 1h (red), 24 h (blue), 72 h (green) and 168 h (purple) and H_2-BTDD (grey) displayed in the area from 4000 to 400 cm^{-1} and from 1800 to 400 cm^{-1}.

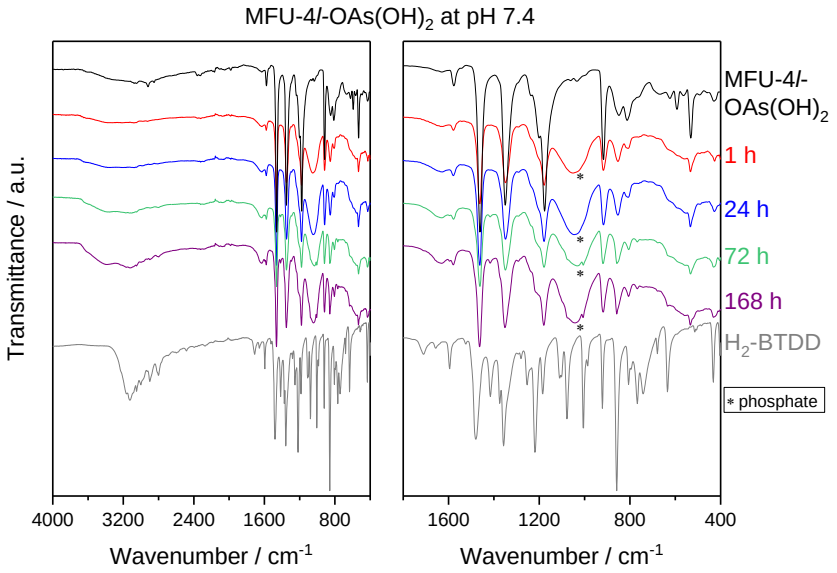

Fig. S13 FTIR spectra of MFU-4*l*-OAs(OH)$_2$ (black) and MFU-4*l*-OAs(OH)$_2$ after the arsenic release studies at pH 7.4 carried out for 1h (red), 24 h (blue), 72 h (green) and 168 h (purple) and H_2-BTDD (grey) displayed in the area from 4000 to 400 cm^{-1} and from 1800 to 400 cm^{-1}.

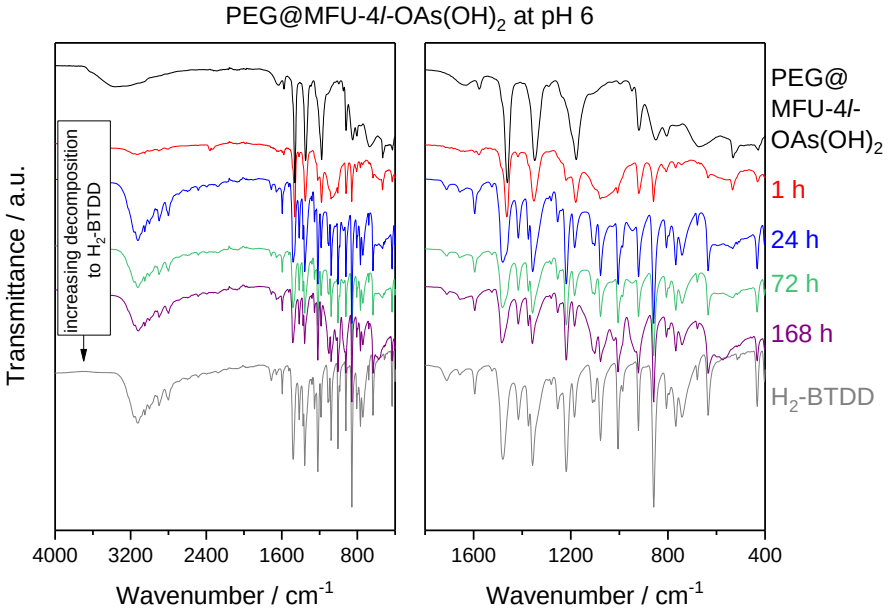

Fig. S14 FTIR spectra of PEG@MFU-4*l*-OAs(OH)$_2$ (black) and PEG@MFU-4*l*-OAs(OH)$_2$ after the arsenic release studies at pH 6 carried out for 1h (red), 24 h (blue), 72 h (green) and 168 h (purple) and H_2-BTDD (grey) displayed in the area from 4000 to 400 cm^{-1} and from 1800 to 400 cm^{-1}.

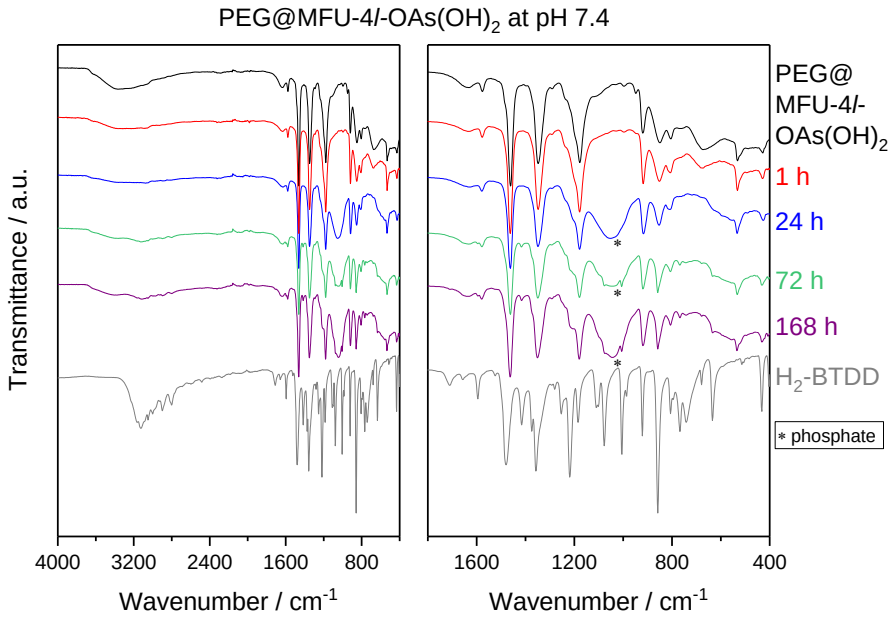

Fig. S15 FTIR spectra of PEG@MFU-4*l*-OAs(OH)$_2$ (black) and PEG@MFU-4*l*-OAs(OH)$_2$ after the arsenic release studies at pH 6 carried out for 1h (red), 24 h (blue), 72 h (green) and 168 h (purple) and H_2-BTDD (grey) displayed in the area from 4000 to 400 cm^{-1} and from 1800 to 400 cm^{-1}.

Thermogravimetric analysis:
(For thermogravimetric analysis of H_2-BTDD and MFU-4*l*-OAs(OH)$_2$ before the release studies see Fig. S5).

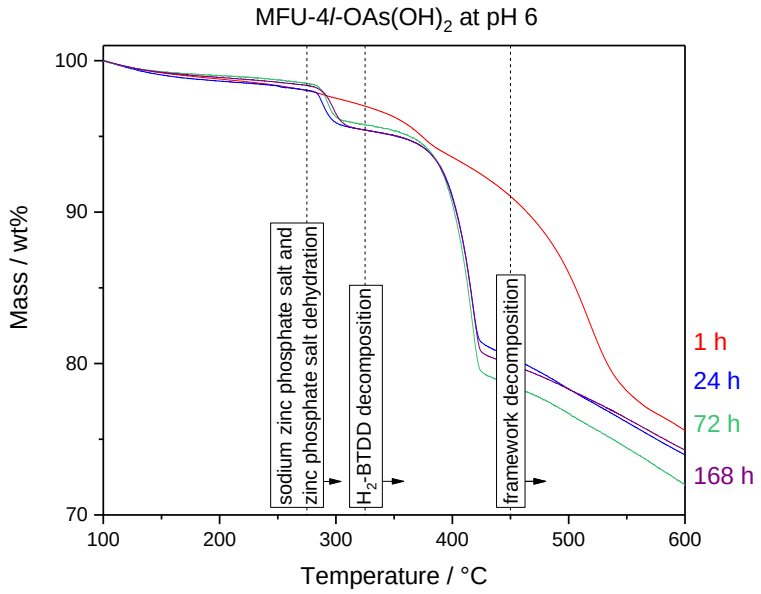

Fig. S16 Thermogravimetric analysis of MFU-4*l*-OAs(OH)$_2$ after the arsenic release studies carried out at pH 6 for 1h (red), 24 h (blue), 72 h (green) and 168 h (purple) (samples were activated at 100 °C for 3h and exposed to a flow of nitrogen gas).

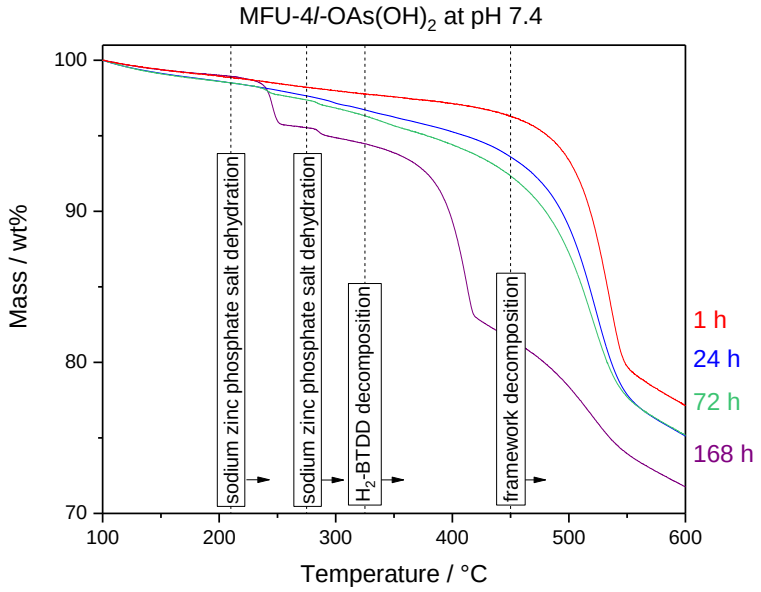

Fig. S17 Thermogravimetric analysis of MFU-4*l*-OAs(OH)$_2$ after the arsenic release studies carried out at pH 7.4 for 1h (red), 24 h (blue), 72 h (green) and 168 h (purple) (samples were activated at 100 °C for 3h and exposed to a flow of nitrogen gas)

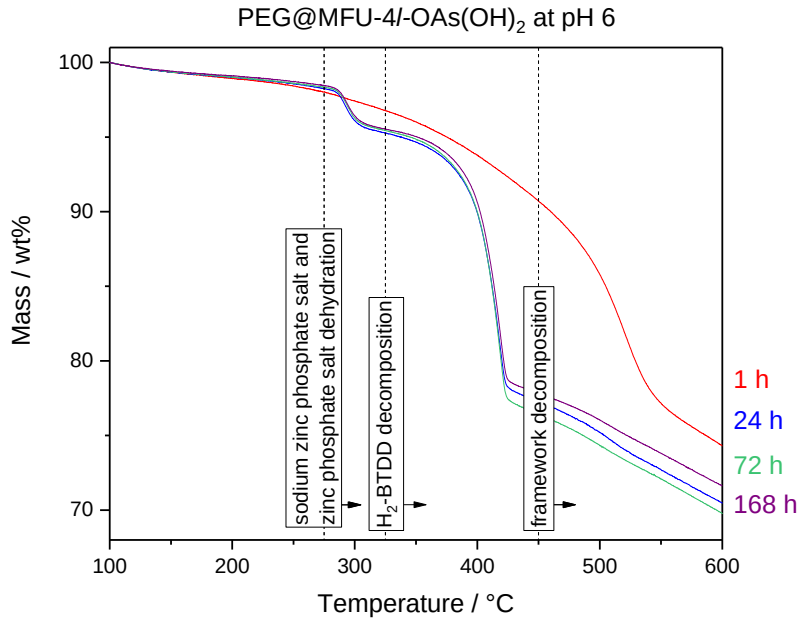

Fig. S18 Thermogravimetric analysis of PEG@MFU-4*l*-OAs(OH)$_2$ after the arsenic release studies carried out at pH 6 for 1h (red), 24 h (blue), 72 h (green) and 168 h (purple) (samples were activated at 100 °C for 3h and exposed to a flow of nitrogen gas).

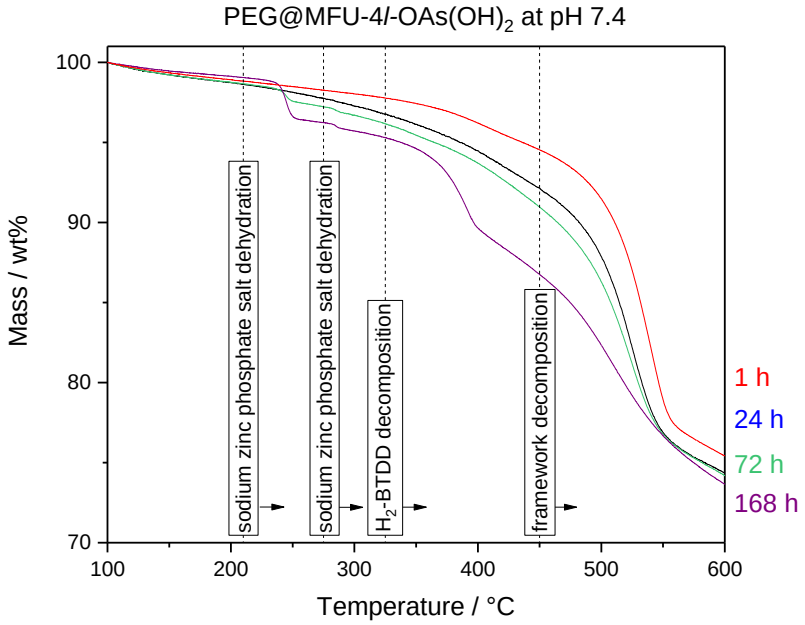

Fig. S19 Thermogravimetric analysis of PEG@MFU-4*l*-OAs(OH)$_2$ after the arsenic release studies carried out at pH 7.4 for 1h (red), 24 h (blue), 72 h (green) and 168 h (purple) (samples were activated at 100 °C for 3h and exposed to a flow of nitrogen gas).

X-ray powder diffraction (XRPD) measurements:

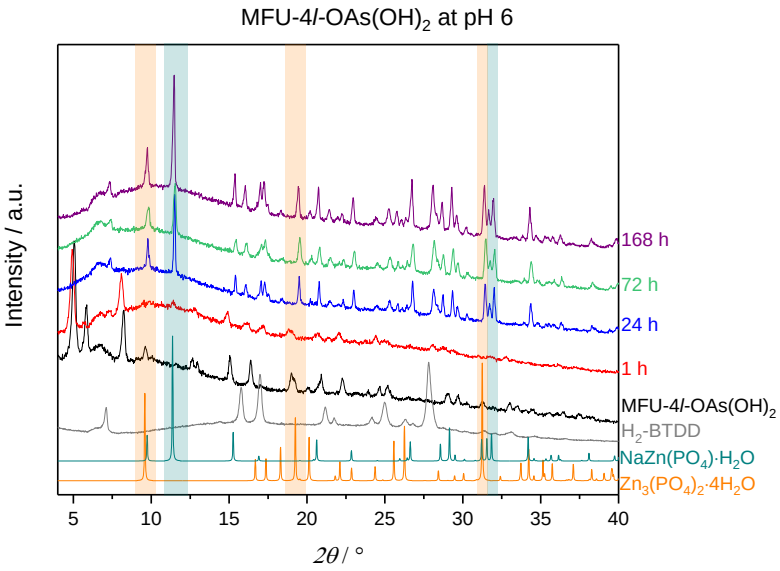

Fig. S20 Comparison of measured XRPD patterns of MFU-4*l*-OAs(OH)$_2$ (black), MFU-4*l*-OAs(OH)$_2$ after the arsenic release studies carried out at pH 6 for 1h (red), 24 h (blue), 72 h (green) and 168 h (purple) and H_2-BTDD (grey) and the calculated XRPD patterns of $Zn_3(PO_4)_2{\cdot}4H_2O$ (orange, CSD: 18145) and $NaZn(PO_4){\cdot}H_2O$ (turquoise, CSD: 81368).

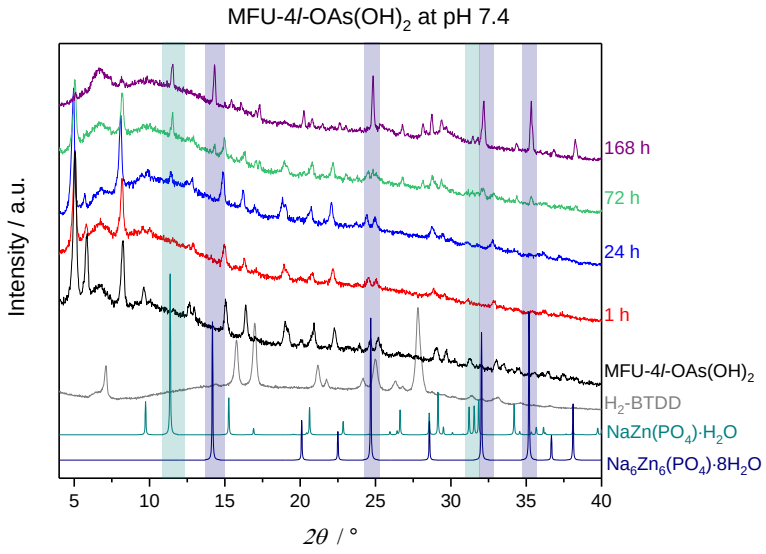

Fig. S21 Comparison of measured XRPD patterns of MFU-4*l*-OAs(OH)$_2$ (black), MFU-4*l*-OAs(OH)$_2$ after the arsenic release studies carried out at pH 7.4 for 1h (red), 24 h (blue), 72 h (green) and 168 h (purple) and H_2-BTDD (grey) and the calculated XRPD patterns of $NaZn(PO_4){\cdot}H_2O$ (turquoise, CSD: 81368) and $Na_6Zn_6(PO_4){\cdot}8H_2O$ (dark blue, CSD: 56499).

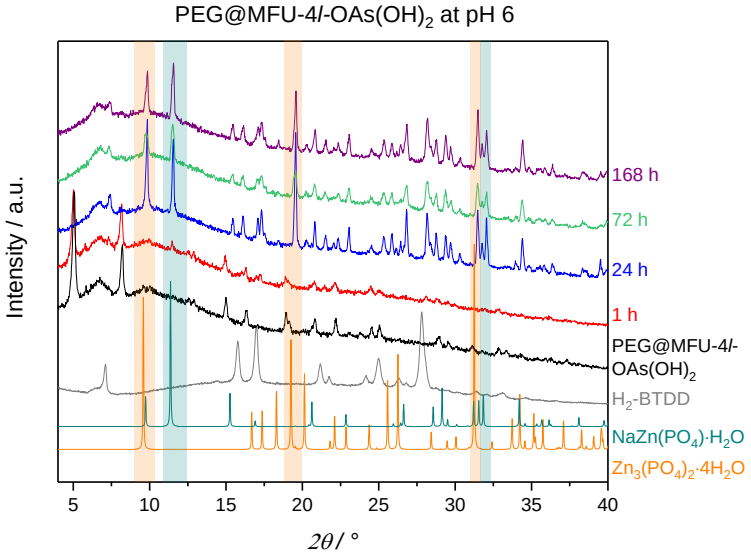

Fig. S22 Comparison of measured XRPD patterns of PEG@MFU-4*l*-OAs(OH)$_2$ (black), PEG@MFU-4*l*-OAs(OH)$_2$ after the arsenic release studies carried out at pH 6 for 1h (red), 24 h (blue), 72 h (green) and 168 h (purple) and H_2-BTDD (grey) and the calculated XRPD patterns of $Zn_3(PO_4)_2{\cdot}4H_2O$ (orange, CSD: 18145) and $NaZn(PO_4){\cdot}H_2O$ (turquoise, CSD: 81368).

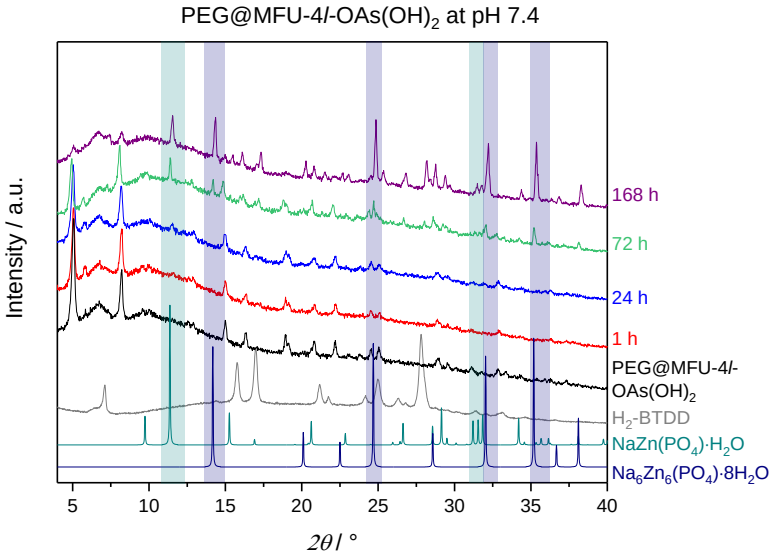

Fig. S23 Comparison of measured XRPD patterns of PEG@MFU-4*l*-OAs(OH)$_2$ (black), PEG@MFU-4*l*-OAs(OH)$_2$ after the arsenic release studies carried out at pH 7.4 for 1h (red), 24 h (blue), 72 h (green) and 168 h (purple) and H_2-BTDD (grey) and the calculated XRPD patterns of $NaZn(PO_4){\cdot}H_2O$ (turquoise, CSD: 81368) and $Na_6Zn_6(PO_4){\cdot}8H_2O$ (dark blue, CSD: 56499).

Cytotoxicity studies

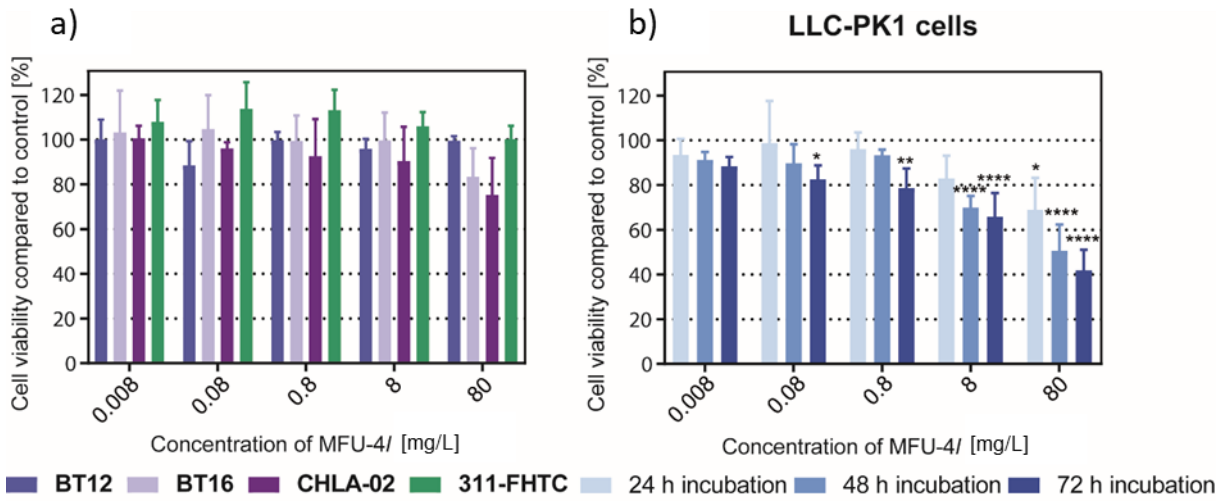

Fig. S24 Cell viability of different ATRT cell lines after 72 h (a) and LLC-PK1 cells after 24 h, 48 h and 72 h (b) incubation with different concentrations of MFU-4*l*. Data are presented as mean ± standard deviation (n ≥ 3). (ANOVA one-way, * indicates $p \leq 0.05$, ** $p \leq 0.01$, **** $p \leq 0.0001$).

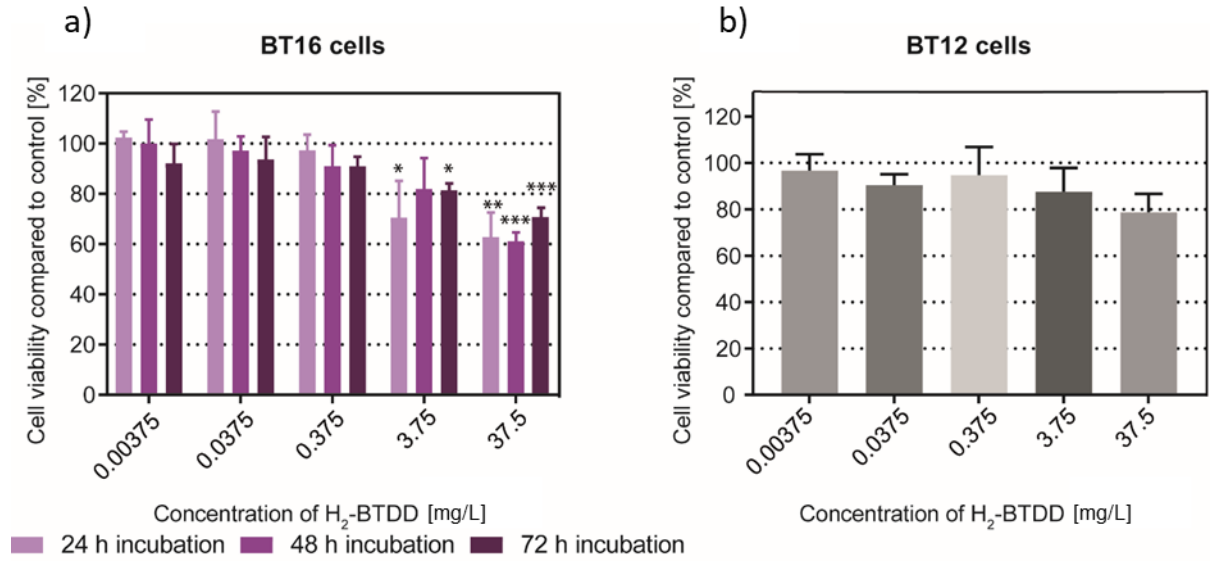

Fig. S25 Cell viability of BT16 cells after 24 h, 48 h, 72 h (a) and BT12 cells after 72 h (b) incubation with different concentrations of H_2-BTDD. Data are presented as mean ± standard deviation (n ≥ 3). (ANOVA one-way, * indicates $p \leq 0.05$, ** $p \leq 0.01$, *** $p \leq 0.001$).

References

1 B. Delley, *J. Chem. Phys.*, 1990, **92**, 508–517.

2 B. Delley, *J. Chem. Phys.*, 2000, **113**, 7756–7764.

3 S. J. Clark, M. D. Segall, C. J. Pickard, P. J. Hasnip, M. I. J. Probert, K. Refson and M. C. Payne, *Z. Kristallog. – Cryst. Mater.*, 2005, **220**, 191.